

Transverse momentum of ionized atoms and diatomic molecules acquired in collisions with fast highly charged heavy ions

V. Horvat* and R. L. Watson

Cyclotron Institute and Department of Chemistry, Texas A&M University, College Station, Texas 77843-3366, USA

(Received 17 May 2013; revised manuscript received 26 June 2013; published 8 August 2013)

Using a recoil-ion momentum spectrometer (RIMS), transverse momenta (q_{\perp}) of recoil atomic and molecular ions emerging from collisions between 2.5-MeV/u Xe^{34+} projectiles and neutral Ne, Ar, CO, N_2 , and O_2 gases were measured as a function of the degree of target ionization. For the molecular targets the resulting distributions of q_{\perp} corresponding to different dissociation channels were separated. Measurements with all the targets were performed under virtually identical conditions so that the results could be directly compared in detail. It was found that the shapes of the q_{\perp} distributions are characterized by single asymmetric peaks and that, at least in the vicinity of their maximum values, they are well described by Weibull functions. Except for the Ar target, the velocities corresponding to the maxima of the q_{\perp} distributions were found to follow (within the uncertainties of the results) a universal function of the target charge-to-mass number ratio for values up to 0.33. For larger charge-to-mass number ratios the results for the molecular targets appear to remain universal, but are slightly lower than the results for the Ne target. A more elaborate scaling was required to obtain a universal function that describes the low-charge-state results for Ne and Ar targets in a similar way. For different dissociation channels of the same parent molecular ion with charge states exceeding $6+$, significant differences were found between the measured q_{\perp} distributions. These differences were ascribed to increases in the ionization potential and to more prominent contributions from target-to-projectile electron transfer for the more asymmetric dissociation channels. For symmetric and nearly symmetric molecular dissociation channels the fragments with combined charge number Q exceeding 9 for N_2 and 10 for O_2 were found to be distributed with a reduced probability at angles close to 90° relative to the beam direction. The magnitude of this effect was found to depend on the number of electrons removed in addition to one half of the number of available electrons ($Q-Z$). On the other hand, for highly asymmetric dissociation channels the angular distributions seem to indicate that the fragments of highly charged molecular ions may be distributed with an enhanced probability at angles close to 90° relative to the beam direction. A slight dependence of the q_{\perp} distribution on molecular orientation was found to be present for the symmetric and nearly symmetric dissociation channels having $Q-Z \geq 0$. The magnitude of this effect also seems to be determined by the value of $Q-Z$.

DOI: [10.1103/PhysRevA.88.022703](https://doi.org/10.1103/PhysRevA.88.022703)

PACS number(s): 34.50.Gb, 34.70.+e

I. INTRODUCTION

The momenta of ions and electrons emerging from collisions between charged projectiles and neutral target atoms or molecules have been topics of interest over the past few decades. Summaries of previous work carried out on this subject and the results obtained are included in several comprehensive review articles covering a broader range of topics [1–5].

However, precise simultaneous measurements of all three individual vector components of momentum for charged recoil ions produced in the collisions became possible more recently, following the development of recoil-ion momentum spectrometers (RIMS) that incorporated fast timing and simultaneous two-dimensional position determination capabilities. The high resolution, high efficiency, and reliability of RIMS is accomplished by combining large-area microchannel plate detectors with delay-line anodes, high-precision time digitizers, and advanced signal-reconstruction algorithms [6]. Continuing improvements in the performance of all these components have paralleled the development of more sophisticated detection systems in which RIMS is an essential component. For

example, in a cold target recoil-ion momentum spectrometer (COLTRIMS) apparatus [3–5] RIMS is used in conjunction with cold targets, which improves accuracy, precision, and resolution in the measurements of recoil-ion momenta, while in a reaction microscope [4,5] RIMS is paired with another device of similar design in order to enable simultaneous measurements of the momenta of recoil ions and ejected electrons.

So far, it has been established [1–5] that ionizing collisions involving fast highly charged heavy ions and neutral atoms having more than two electrons occur predominantly at large impact parameters and may result in single, double, or multiple ionization of the target atoms, thus turning them into charged recoil ions. Ionization of the target atoms is predominantly due to pure ionization, in which the projectile charge does not change. The resulting recoil-ion charge distribution is a steep monotonically decreasing function of charge [7], while the recoil-ion transverse momentum q_{\perp} (perpendicular to the momentum of the incoming projectile) is relatively small for low-charged recoil ions (i.e., no more than a few atomic units), but increases rapidly as a function of recoil-ion charge [1–5]. This increase is a consequence of the fact that Coulomb interaction between the projectile and the recoil ion (after its formation) is stronger when the recoil-ion charge is higher and when the impact parameter is smaller. These

*Corresponding author: V-Horvat@tamu.edu

two causes are related, since recoil ions with higher charge are generally produced in collisions characterized by smaller impact parameters.

The production of very high recoil-ion charge states at very small impact parameters is increasingly due to ionization accompanied by single-, double-, or multiple-electron transfer from the target to the projectile or projectile single-, double-, or multiple-electron loss. The recoil-ion charge distributions resulting from these processes are generally bell shaped [7].

Published results of measurements of q_{\perp} distributions for multiply charged recoil ions are very scarce. For the strong-interaction regime, which is the focus of this paper, one notable contribution includes the work of Unverzagt *et al.* [8], involving a 5.9-MeV/u U^{65+} beam and a neon gas target, in which q_{\perp} distributions are shown for recoil ions having charge states up to $5+$. The results were found to be in excellent agreement with n -body classical trajectory Monte Carlo (n CTMC) calculations folded with the thermal momentum distribution of the target gas. Likewise, Jardin *et al.* [9] used 6.7-MeV/u Xe^{44+} ions and an argon target to measure q_{\perp} distributions for recoil ions with charge state up to $7+$. Furthermore, Frohne *et al.* [10], bombarded neon target atoms with 19-MeV F^{9+} projectiles and obtained q_{\perp} distributions for recoil ions with charge states up to and including $5+$ for the pure ionization process, and up to and including $7+$ ($8+$) for collisions in which the outgoing projectile charge state was $8+$ ($7+$), respectively. It was found that the agreement between the measurements and the n CTMC calculations worsened as the recoil-ion charge increased and/or as the outgoing projectile charge decreased.

Despite the best efforts of the present authors, reports of measured q_{\perp} distributions in strong-interaction collisions between fast highly charged heavy ions and molecules having more than two electrons could not be found. Presumably, the transverse momentum of molecular ions emerging from the collisions should have a distribution similar to that expected for ionized atomic targets having comparable charge-to-mass ratio, as long as the size of the molecule is much smaller than the impact parameter. However, this may not hold true for small-impact-parameter collisions that result in double or multiple target ionization, which in turn leads to the dissociation of molecules, predominantly into positively charged fragments. In order to provide a detailed comparison of the shapes of the q_{\perp} distributions in these two cases, the measurements require good statistics, which becomes critical at higher charge states of the recoil (atomic) ions and recoil (parent) molecular ions, commonly referred to as *the recoils*. It should be noted that in this work the term “recoil ion” or “recoil” will not be used to refer to a molecular fragment.

The main goal of the work presented here is to measure, study, and compare the distributions of q_{\perp} for atoms and diatomic molecules having more than two electrons at the time of collision with fast heavy ions. In order to facilitate the comparisons, the measurements were performed under virtually identical conditions for all targets. This means that the apparatus was set to accommodate the stricter requirements of the measurements involving molecular targets and was not optimized further for the measurements involving atomic targets by lowering the extraction field. This was clearly a disadvantage for the latter case, but good results were obtained

nevertheless, due to the fact that transverse momentum of recoil atomic ions in the collision regime studied here is relatively large and that the large size of the recoil detector used in the present experiment provided for high acceptance of correlated energetic molecular fragments even at a relatively low extraction field.

II. EXPERIMENT

The setup used in the present work has been described in detail in a previous publication [11]. Briefly, a beam of 2.5-MeV/u Xe^{13+} ions was extracted from the Texas A&M K500 superconducting cyclotron and directed through an aluminum stripper foil. Ions of Xe^{34+} were separated from the resulting distribution of Xe ions in various charge states by means of a bending magnet and then transported in the parallel-beam mode to the target chamber. There the beam passed through two 1-mm-diameter collimators before entering the spectrometer, where it was crossed with a target gas jet that had density low enough to ensure single-collision conditions. The ion beam then proceeded into a postcollision charge-state analysis system consisting of a dipole magnet and two detectors. A plastic scintillator coupled to a photomultiplier tube was used when the magnet was not energized to mark the time of arrival of the beam particles, whereas a one-dimensional position-sensitive microchannel plate detector with a resistive anode was used when the magnet was energized to measure the outgoing beam charge-state distribution.

A typical example of the measured outgoing beam charge-state distribution is shown in Fig. 1. It was found that under the present experimental conditions, the pure ionization mechanism is responsible for more than 98% of collisions.

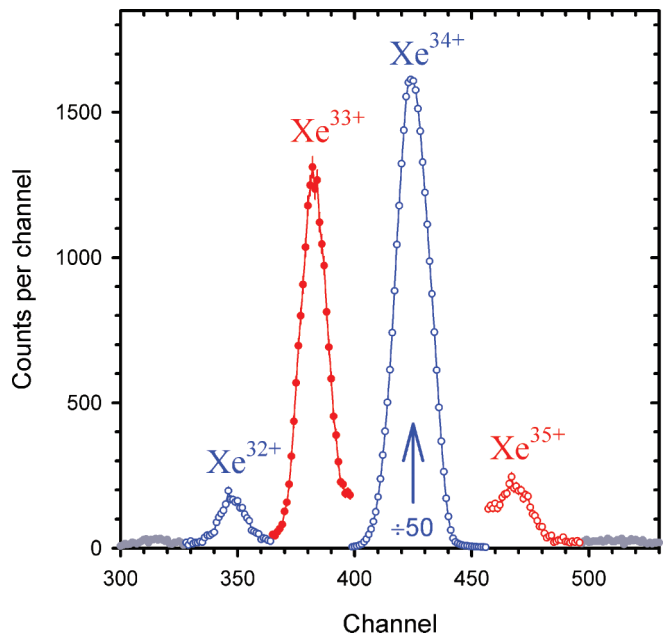


FIG. 1. (Color online) Measured charge-state distribution of 2.5-MeV/u Xe^{34+} ions after passing through a carbon monoxide gas jet. The counts in the region covered by the Xe^{34+} peak are shown divided by 50. No significant difference in the distribution was found in the measurements with the other targets.

The next most important contribution of about 1.3% is from ionization accompanied by a single-electron transfer to the projectile, while ionization accompanied by a projectile single-electron loss accounts for only about 0.3% of the collisions. No significant difference in the distribution was found in the measurements with different gases.

Charged recoils and molecular fragments were accelerated by a uniform electric field, produced by applying a 1554-V bias over the length of 61 mm, and then drifted in a field-free region having a length of 122 mm. Upon exit, the ions were further accelerated toward the front microchannel plate (MCP) of the recoil or molecular-fragment detector located 6 mm away and biased at -2600 V.

The recoil or molecular-fragment detector consists of a triple set (Z stack) of MCPs (RoentDek HEX80). Fast timing signals marking the arrival of recoils or molecular fragments were obtained from the back side of the MCP stack and together with the signals from the beam particle detector were used to determine the times of flight of the recoils.

The MCP stack is backed by a hexanode consisting of three layers of delay-line arrays [6] and was used to measure the two impact-position coordinates (x and y) of each ion. From the time of flight and coordinates x and y it is possible to determine the momentum that each positively charged atomic or molecular ion acquires immediately after the collision with the beam particle and/or the momentum that each positively charged molecular fragment acquires due to molecular dissociation [11]. Arrival times of all the signals were measured by an eightfold multihit time-to-digital converter (TDC) (RoentDek TDC8HP) interfaced to a fast personal computer running a data acquisition and analysis program (RoentDek CoboldPC).

The analysis is based on a right-handed Cartesian reference frame having its origin at the front-plate center of the recoil or molecular-fragment detector, such that the beam propagates in the positive x direction, while the ions hit the detector having a negative z component of velocity. (In the present setup the x and z axes are both horizontal). The spectrometer was carefully calibrated regarding its time and position scales, efficiency, and acceptance of the correlated molecular-fragment pairs [11].

III. DATA ANALYSIS

For a collision-induced breakup of a molecule into two positively charged fragments with masses m_1 and m_2 , times of flight T_1 and T_2 , and impact-position coordinate pairs (x_1, y_1) and (x_2, y_2) , respectively, the components $p_x(1)$, $p_y(1)$, $p_z(1)$, and $p_x(2)$, $p_y(2)$, $p_z(2)$ of the molecular-fragment momenta acquired due to the breakup can be determined as described and explained in Ref. [11]. Using the same notation, the recoil molecular ion transverse momentum q_\perp and its Cartesian components q_z and q_y can be determined using the expressions

$$q_z = p_z(1) + p_z(2), \quad (1)$$

$$q_y = m_1(y_1 - y_c)/T_1 + m_2(y_2 - y_c)/T_2, \quad (2)$$

and

$$q_\perp = (q_y^2 + q_z^2)^{1/2}, \quad (3)$$

where y_c is the y coordinate of the center of the interaction region [11].

If the target ionized in the collision with the projectile is atomic or if it is molecular but does not dissociate, then Eq. (3) still applies, but respectively, Eqs. (1) and (2) are replaced by

$$q_z = p_z \quad (4)$$

and

$$q_y = m(y - y_c)/T. \quad (5)$$

Here m , T , and y , respectively, are the mass, the time of flight, and the impact-position y coordinate of the recoil.

The two main sources of systematic error affecting the q_\perp distributions are expected to be (i) the finite beam width in the y direction (the contribution from the finite beam width in the z direction is negligible due to the time-focusing property of the spectrometer) and (ii) the thermal spread in the y and z velocity components of the atomic or molecular target cores at the time of collision. These sources of systematic error effectively increase the widths of the measured q_y and q_z distributions, which in turn results in the increased width and upward shift of the centroid of the measured q_\perp distribution. Since the systematic error is roughly the same for all measured values of q_y and q_z , its effect on the value of q_\perp is most significant when both q_y and q_z are small. For large values of q_y and q_z the effect is *relatively* small.

Respectively, if q_y is small (large), q_z is not necessarily small (large) as well. However, if the q_\perp distribution peaks at a low value of q_\perp , then most contributions come from the combinations in which q_y and q_z are both small. Consequently, the peak value of the q_\perp distribution is significantly overestimated. On the other hand, if the q_\perp distribution peaks at a high value of q_\perp , then, in most cases, at least one of the two (q_y or q_z) is large and so the relative effect of the systematic error on the deduced value of q_\perp is rather small.

The systematic error can be reduced by (i) reducing the beam width (primarily by using collimators with smaller apertures) and (ii) reducing the gas jet temperature (primarily by precooling the gas). In the present work the beam width was chosen based on the goals and the conditions of the measurements, most importantly the amount of time allocated to the experiment and the desired quality of the event statistics. The gas jet was not precooled for practical reasons. However, it has been shown that the momentum resolution achieved with a skimmer-collimated effusive gas jet (used here) is comparable to that achieved with a cooled gas cell [3]. The actual q_\perp resolution was estimated based on the measured q_\perp distribution as being better than 5 a.u. This will be elaborated on in Sec. IV B.

The q_\perp resolution also can be improved by reducing the extraction field, thus increasing the time of flight and the y range for all the recoils and molecular fragments. However, in this work, the times of flight were limited by the desire to have high acceptance for correlated energetic molecular fragments and virtually identical experimental conditions for the measurements with both atomic and molecular targets.

On the other hand, those distributions that are expected to be broad and smooth and not to extend to low values of q_\perp are also not expected to be significantly affected by the two sources of systematic error listed above. An example of such a case is

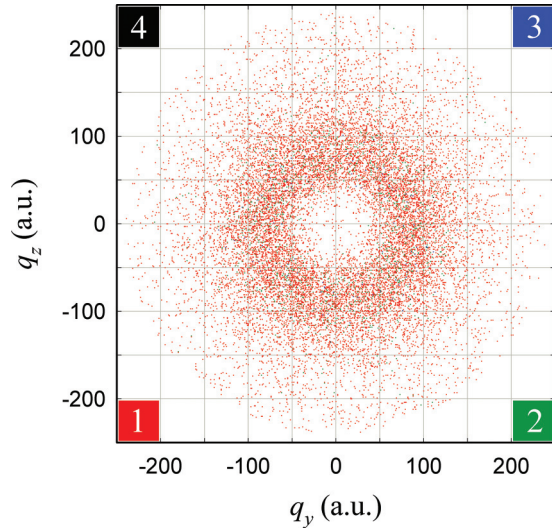


FIG. 2. (Color online) Two-dimensional histogram of the transverse momentum components q_y and q_z for Ar^{12+} ions produced in the collisions of neutral argon atoms with 2.5-MeV/u Xe^{34+} ions. The bin size is 1 a.u. \times 1 a.u., while the color scheme used to indicate the number of counts per bin is shown by the colored tiles located at the corners of the graph.

given in Fig. 2, which shows a two-dimensional histogram of q_y versus q_z for Ar^{12+} ions, featuring almost complete absence of events at small values of q_{\perp} and a wide single-peak-profiled ring centered at the origin. The lack of events at small values of q_{\perp} implies it is unlikely that a projectile removes as many as twelve electrons from an argon atom in a collision in which the recoil ion acquires only a small transverse momentum. It also implies that Ar^{12+} ions are unlikely to be produced in collisions at impact parameters that are large compared to the size of the projectile ion and/or the target atom.

It should be noted that transverse momenta acquired in the collision by the ejected electrons and the projectile have not been measured in this work. However, the law of conservation of momentum requires that the total transverse momentum is zero. Therefore, the distribution of the measured quantity q_{\perp} (i.e., the recoil transverse momentum) is affected by the postcollision distribution of transverse momenta of the ejected electrons and the projectile. In other words, q_{\perp} is sensitive to the full dynamics of the collision [2,8].

IV. RESULTS AND DISCUSSION

A. Comparison between q_{\perp} distributions for related molecular dissociation channels

Since in the strong-interaction regime the duration of a collision (on the order of 10^{-17} s in the present case) is typically much shorter than the target relaxation time (on a time scale of 10^{-14} s in this work), it can be expected that target relaxation is virtually unaffected by the projectile. Consequently, in the case of ionization of a diatomic molecule by a fast projectile, followed by the molecular dissociation into two positively charged fragments having charge numbers Q_1 and Q_2 , it is expected that the q_{\perp} distributions are essentially the same for all dissociation channels corresponding to the same combined fragment charge number $Q = Q_1 + Q_2$.

This is confirmed to be true for values of $Q < 7$, as demonstrated in Fig. 3 for the case of carbon monoxide molecular dissociation. A similar kind of confirmation was obtained for the corresponding N_2 and O_2 dissociation channels. The observed upward shift of the distributions as Q increases is due to the fact that a parent molecular ion with a higher value of Q is more likely to be produced in a collision at a smaller impact parameter, which in turn is more likely to result in a larger transverse momentum of the target core due to the increased Coulomb interaction between these two collision partners. This effect will be referred to as the Q shift in the text that follows.

However, for $Q \geq 7$, it was found that a more asymmetric dissociation channel (i.e., one corresponding to a larger value of $|Q_1 - Q_2|$) has a larger Q shift compared to a less asymmetric dissociation channel (i.e., one corresponding to a smaller value of $|Q_1 - Q_2|$). The absolute difference between these Q shifts was found to increase as Q increases. This is demonstrated in Fig. 4 for the case of N_2 molecular dissociation. The same conclusion can be drawn for the distributions (not shown) in the case of O_2 molecular dissociation. Even the bottom plot of Fig. 3 displays a hint of this effect, which will be referred to as the ΔQ split in the text that follows.

Moreover, Fig. 4 also shows that for $Q = 9$ and 10, the ΔQ splits are much larger than those observed for $Q = 7$ and 8. Considering that the two more asymmetric dissociation channels for $Q = 9$ and 10 include a hydrogenlike N^{6+} ion, this effect is presumably due to the fact that in order to remove a tightly bound nitrogen K -shell electron in addition to other more loosely bound electrons, a significant increase in the ionization potential must be overcome, for which the average impact parameter must decrease more drastically than is required for the removal of a less tightly bound electron. The same argument also helps explain why the less asymmetric dissociation channel is the dominant one.

For $Q = 9$ and 10, the q_{\perp} distributions for the dissociation channels involving an N^{6+} ion, compared to the other two distributions, also have significantly longer tails, well beyond what could be expected based on the overall upward shift of the distributions (the ΔQ split), which includes the upward shift of the distributions' peak values. This additional effect (which is also apparent in Fig. 4 for $Q = 8$) has a different character than that of the ΔQ split and will be referred to as the tail effect in the text that follows. The onset of the tail effect at $Q = 8$ is most-likely related to the increased importance of a different ionization mechanism involving target-to-projectile electron transfer, which is known to become increasingly important for the production of highly charged recoils [7] and also for the removal of tightly bound target electrons. Therefore, the tail effect could be explained by the difference between the impact parameter distribution of pure ionization (which in the present case is dominant for $Q \leq 7$) and that of ionization accompanied by electron transfer from the target to the projectile (which in the present case becomes apparent at $Q \geq 8$ when the target starts losing its tightly bound electrons).

The Q shift and the onset of the tail effect also can be observed in the case of atomic targets, as shown in Fig. 5. A significant enhancement at higher values of q_{\perp} occurs at the crossover from heliumlike to hydrogenlike neon ions and from carbonlike to boronlike argon ions. In both cases, production

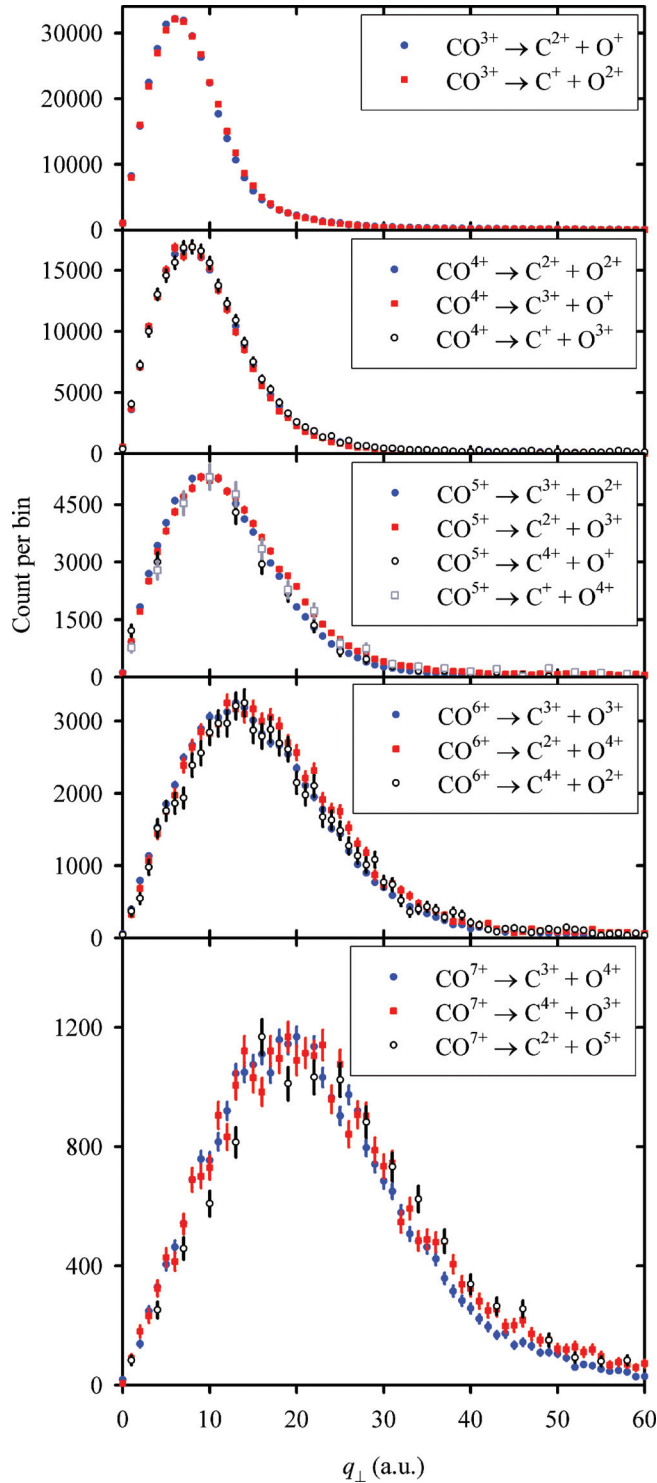


FIG. 3. (Color online) Comparison of the q_{\perp} distributions for dissociation channels corresponding to the same carbon monoxide parent molecular ion, which is assumed to have charge number equal to the combined fragment charge numbers. In each plot, the number of counts per bin as indicated on the vertical axis scale applies to the dominant dissociation channel (i.e., one that is listed first in the legend). Distributions for the remaining dissociation channels in each plot were scaled so that their maximum values match that of the corresponding dominant dissociation channel. The bin size is 3 a.u. for $\text{CO}^{7+} \rightarrow \text{C}^{2+} + \text{O}^{5+}$ and 1 a.u. for the remaining dissociation channels. The error bars shown are purely statistical.

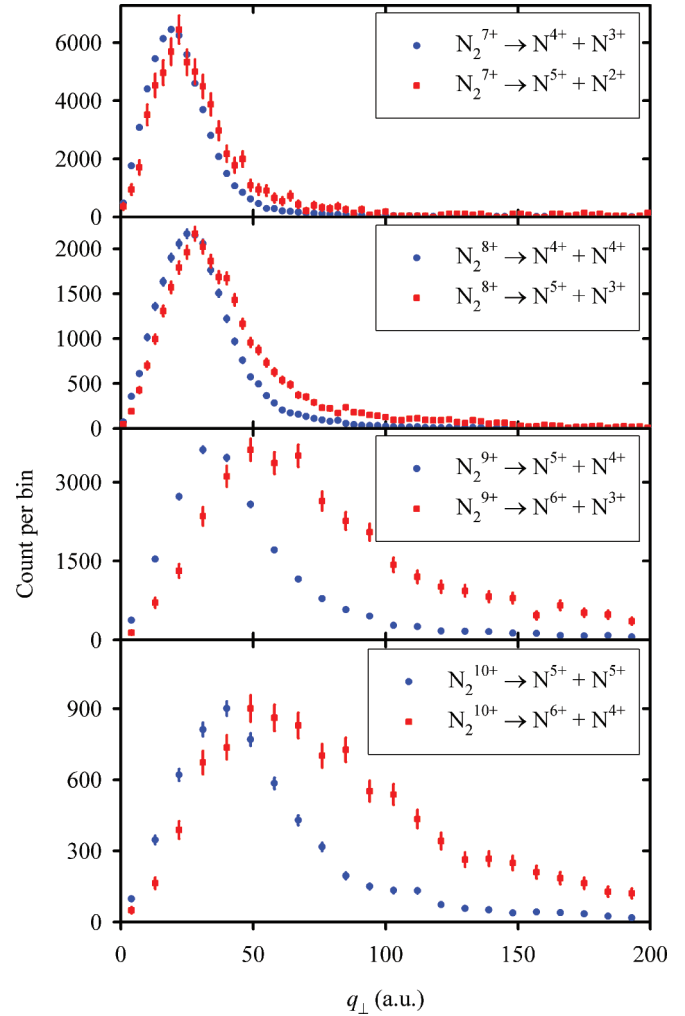


FIG. 4. (Color online) Comparison of the q_{\perp} distributions for dissociation channels corresponding to the same N_2 parent molecular ion, which is assumed to have charge number equal to the combined fragment charge numbers. In each plot, the number of counts per bin as indicated on the vertical axis scale applies to the dominant dissociation channel (i.e., one that is listed first in the legend). Distributions for the remaining dissociation channels in each plot were scaled so that their maximum values match that of the corresponding dominant dissociation channel. The bin size is 3 a.u. for N_2^{7+} and N_2^{8+} and 9 a.u. for N_2^{9+} and N_2^{10+} parent molecular ions. The error bars shown are purely statistical.

of the latter ion involves the removal of an electron from the next inner subshell (K for Ne and L_2 for Ar).

In experiments with atomic targets in which q_{\perp} distributions are measured in coincidence with the outgoing projectile charge, contributions from pure ionization are separated from those that involve electron transfer, and so the tail effect can be observed at even lower recoil-ion charge states. For example, compare the q_{\perp} distributions for Ne^{4+} or Ne^{5+} recoil ions in collisions involving double-, single-, and no-electron capture by the projectile, as shown in Fig. 7 of Ref. [10]. Therefore, we can conclude that the root cause of the tail effect is the increased contribution from the electron transfer mechanism and its associated impact parameter distribution,

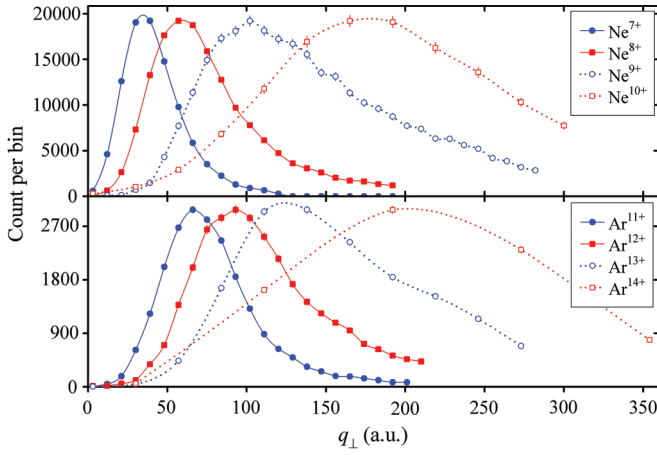


FIG. 5. (Color online) Distributions of q_{\perp} for the highest recoil charge states obtained in the measurements with neon and argon targets. The error bars shown are purely statistical. The lines are drawn to guide the eye. In each plot, the number of counts per bin as indicated on the vertical axis scale applies to the most-abundant recoil ion (having lowest charge and listed first in the legend). Distributions for the remaining recoil ions in each plot were scaled so that their maximum values match that of the corresponding most-abundant recoil ion. The bin size is 9 a.u. for Ne^{7+} , Ne^{8+} , Ar^{11+} , and Ar^{12+} , 27 a.u. for Ne^{9+} , Ne^{10+} , and Ar^{13+} , and 81 a.u. for Ar^{14+} .

which apparently extends to lower impact parameters than that of pure ionization.

In the strong-interaction regime, the effects described and explained above (i.e., the Q shift, the ΔQ split, and the tail effect), are expected to have a very weak dependence on the projectile species, projectile charge, and projectile energy. This is because, in the strong-interaction regime, a certain interaction strength is required to produce a given state of target ionization and excitation. A selected final outcome (following the relaxation) also implies a selected corresponding range of the interaction strength. However, interaction strength is determined by the projectile charge and velocity, as well as the impact parameter, and so the same interaction strength can be produced at different combinations of these parameters, i.e., by different projectile species at different energy and different charge, provided that the impact parameter in each case has the required matching value.

B. Comparison between q_{\perp} distributions for CO and N_2

The q_{\perp} distributions for N_2 and CO molecular ions dissociating into positively charged fragments, as a function of the combined fragment charge number $Q \leq 7$, are compared in Fig. 6, in which contributions from dissociation channels corresponding to the given combined charge are added together. Apparently, there is hardly any significant difference between any two distributions shown in the same plot. This can be expected based on the fact that the two molecules have the same combined atomic mass number and the same combined atomic number. However, N_2 and CO also have significantly different distributions of their excited states, which is evidenced by the significantly different kinetic-energy release (KER) spectra for doubly and triply charged molecular ions, as shown in Figs. 3 and 5 of Ref. [11]. This implies that, as long as tightly bound

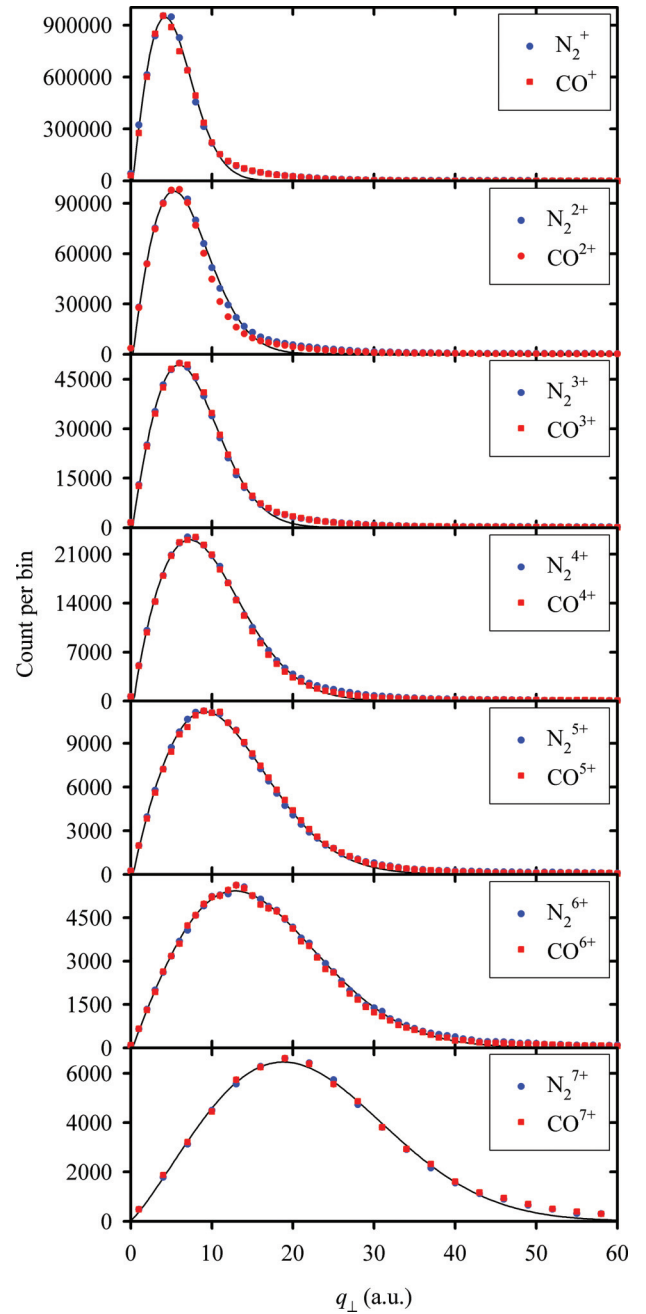


FIG. 6. (Color online) Comparison of the q_{\perp} distributions for N_2 and CO molecular ions dissociating into positively charged fragments, as a function of the combined fragment charge number. Contributions from the dissociation channels corresponding to the given combined charge were added together. In each plot, the number of counts per bin as indicated on the vertical axis scale applies to the case of N_2 . The distribution corresponding to CO in each plot was scaled so that the two maximum values match. The bin size is 3 a.u. for CO^{7+} and N_2^{7+} and 1 a.u. for the remaining parent molecular ions. The statistical error bars are not visible because they are smaller than the symbol size. The parent molecular ion's charge state listed in the legend is assigned the value equal to the combined fragment charge number (thus systematically but consistently neglecting possible effects of autoionization). For completeness, also included is a plot showing the q_{\perp} for nondissociated N_2^{2+} and CO^{2+} molecular ions. The solid lines represent the overall fit of the distributions for N_2^{Q+} (parent) molecular ions ($Q \leq 7$) using Weibull functions.

electrons are not removed, or as long as pure ionization is the dominant mechanism for electron removal, the electronic or molecular structure of the target does not significantly affect the q_{\perp} distribution.

Also included in Fig. 6 is a plot showing the q_{\perp} distributions for nondissociated N_2^+ and CO^+ molecular ions, which shows that the transverse momentum resolution in the present work is about 5 a.u. or better, as expected considering that a skimmer-collimated effusive gas jet was used [3].

All of the measured q_{\perp} distributions were fitted with a four-parameter Weibull function in the form

$$y = A|x|^{c-1} \exp(-|x|^c), \quad (x > 0), \quad (6)$$

where

$$A = ak^{-k} \exp(k), \quad (7)$$

$$x = k^{1/c} + (q_{\perp} - q_{\perp}^0)/b, \quad (8)$$

and

$$k = (c - 1)/c, \quad (9)$$

while a , b , c , and q_{\perp}^0 are the parameters of the fit. The results for N_2^{Q+} (parent) molecular ions ($Q \leq 7$) are shown by the solid lines in Fig. 6. Apparently, Weibull functions represent the shapes of the q_{\perp} distributions very well, with only minor discrepancies at the tail for $Q \leq 3$. A similar quality of fit was obtained for all the other q_{\perp} distributions. By restricting the region of fit to the area around the peak of the distribution (typically the region covered by the full width at half maximum), best estimates of the peak positions q_{\perp}^0 could be determined precisely and in a consistent way.

C. Angular distributions and correlation between q_{\perp} and the orientation of the target molecules at the time of collision

Since periods of rotation for the diatomic molecules used in this work are on the order of 10^{-12} s, while molecular fragmentation resulting from Coulomb explosions of the multicharged molecular ions occurs on a much shorter time scale (of 10^{-14} s), it may be assumed that the orientation of the molecular axis remains unchanged between the time just prior to the collision and the end of the dissociation process. Therefore, it also may be assumed that orientation of the target molecule at the time of collision is defined by the momentum vector of its charged fragments during dissociation.

It is expected that orientation of the target molecule at the time of collision does not affect q_{\perp} as long as the impact parameter is significantly larger than the size of the molecule. This condition is fulfilled for the majority of collisions that result in the removal of only a small number (or fraction) of electrons from the target. On the other hand, most close collisions result in the removal of a large fraction of electrons from the target and the process might be expected to have some dependence on the molecular orientation. Specifically, if the target molecule is initially oriented in the longitudinal direction, the impact parameters for two atomic centers are similar and the collision is expected to result in a symmetric or nearly symmetric charge distribution between the atomic centers of the molecule. On the other hand, if the target

molecule is initially oriented in the transverse direction, the impact parameters for two atomic centers are significantly different and the collision is expected to result in a highly asymmetric charge distribution. Therefore, the dissociation channels characterized by highly asymmetric charge distributions between the atomic centers are expected to have angular distributions that are enhanced in the transverse direction, while the dissociation channels characterized by symmetric or nearly symmetric charge distributions are expected to have angular distributions that are suppressed in the transverse direction.

As expected, no conclusive evidence was found of anisotropy in the distributions of fragment pairs from low-charged molecular ions. However, for the symmetric and the nearly symmetric dissociation channels (i.e., those corresponding to $|Q_1 - Q_2| \leq 1$), the fragments with combined charge number Q exceeding 9 for N_2 and 10 for O_2 were found to be distributed with a reduced probability at angles α close to 90° relative to the beam direction, as illustrated in Fig. 7. Furthermore, the effect was found to become more significant as Q increases. Interestingly, the magnitude of the effect seems to depend on Δn , the number of electrons removed *in addition* to one half of the number of available electrons ($\Delta n = Q - Z$). Consequently, the plots shown in Fig. 7 are selected and arranged so that each row corresponds to a given number $Q - Z$, where Z is the atomic number of nitrogen (in the first column) or oxygen (in the second column).

For highly asymmetric dissociation channels (i.e., those corresponding to $|Q_1 - Q_2| \geq 2$) usable experimental results (selectively shown in Fig. 8) are limited to the cases with $Q < 11$, due to the fact that the production cross section decreases as Q increases and the fact that the predominant dissociation channels are symmetric or nearly symmetric. Also, the highest-observed fragment charge number was 6. A higher fragment charge would require K -shell ionization of oxygen or double K -shell ionization of nitrogen, for which the cross section is relatively low due to the relatively high binding energy of the K electrons. Nevertheless, the angular distributions shown in Fig. 8 for $Q = 9$ are slightly different than those shown in Fig. 7 for the same value of Q , indicating that the fragments of highly charged molecular ions may be distributed with an *enhanced* probability at angles α close to 90° relative to the beam direction.

The onset of the observed angular anisotropy may also be affected by the charge redistribution between the molecular fragments that may occur during dissociation and by autoionization, which is more likely to affect the fragment having lower charge (i.e., more electrons). Both effects are likely to lead to charge equalization, which in effect makes an event from a more asymmetric dissociation channel appear in a less asymmetric (and more prominent) dissociation channel. Due to the apparent complementary properties of the angular distributions for these two dissociation channels (as described above), such events could make the angular distribution of the latter dissociation channel appear less anisotropic, thus shifting the onset of the observed anisotropy to higher values of Q .

As Q becomes large, autoionization becomes less likely because of the smaller number of available electrons and higher electronic binding energies, while charge redistribution

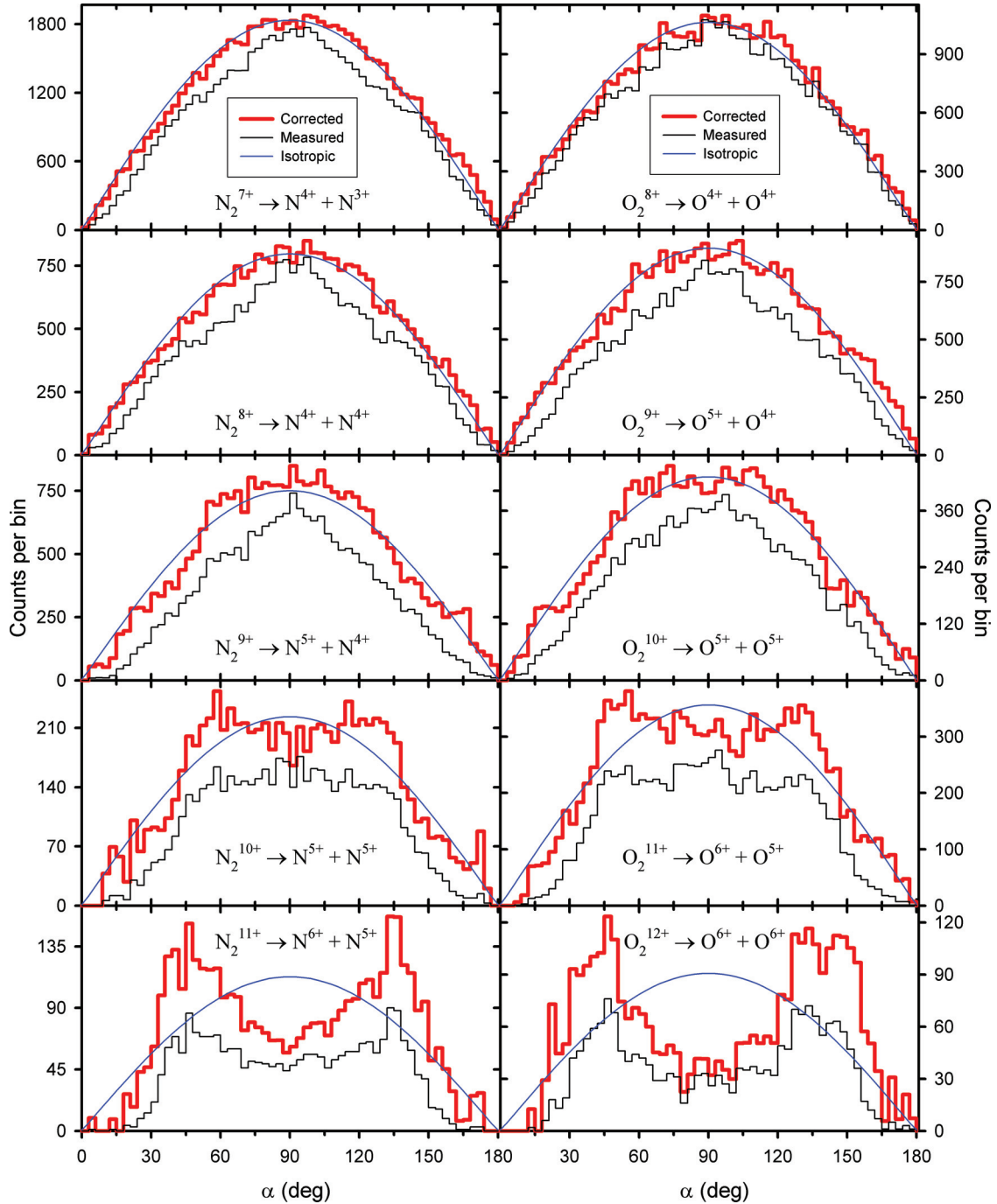


FIG. 7. (Color online) Distributions of the numbers of correlated charged N_2 and O_2 molecular-fragment pairs for the dissociation channels as indicated by the labels, shown as a function of angle α between the molecular axis at the time of collision and the beam direction, at bin size of 3° . The thin (black) line represents the histogram of raw data, while the histogram shown with the thick (red) line is obtained by correcting the raw data for efficiency and fragment-pair acceptance of the apparatus, as described in detail in Ref. [11]. The smooth thin (blue) line shows the ideal isotropic distribution for the corrected total number of events. The N_2 and O_2 molecular ions in each row have the same value of Δn .

may require tunneling of the electrons through the potential barrier between the atomic centers, which occurs with a drastically reduced probability. It can be estimated that the potential barrier of an electron transferring from N^{3+} to N^{6+} (about 80 eV) is only slightly higher than the ionization potential of N^{3+} (about 77 eV), which would imply that charge redistribution is unlikely for $Q > 9$. The reduced probability

of charge equalization for $Q > 9$ coincides with the seeming onset of the deviations from an isotropic distribution, as shown in Figs. 7 and 8.

The effect of molecular orientation on q_\perp distributions was found to be small. Consequently, the angular scale was reduced to only two bins; one covering $60^\circ \leq \alpha \leq 120^\circ$ and the other covering the remainder of the angular range, so that

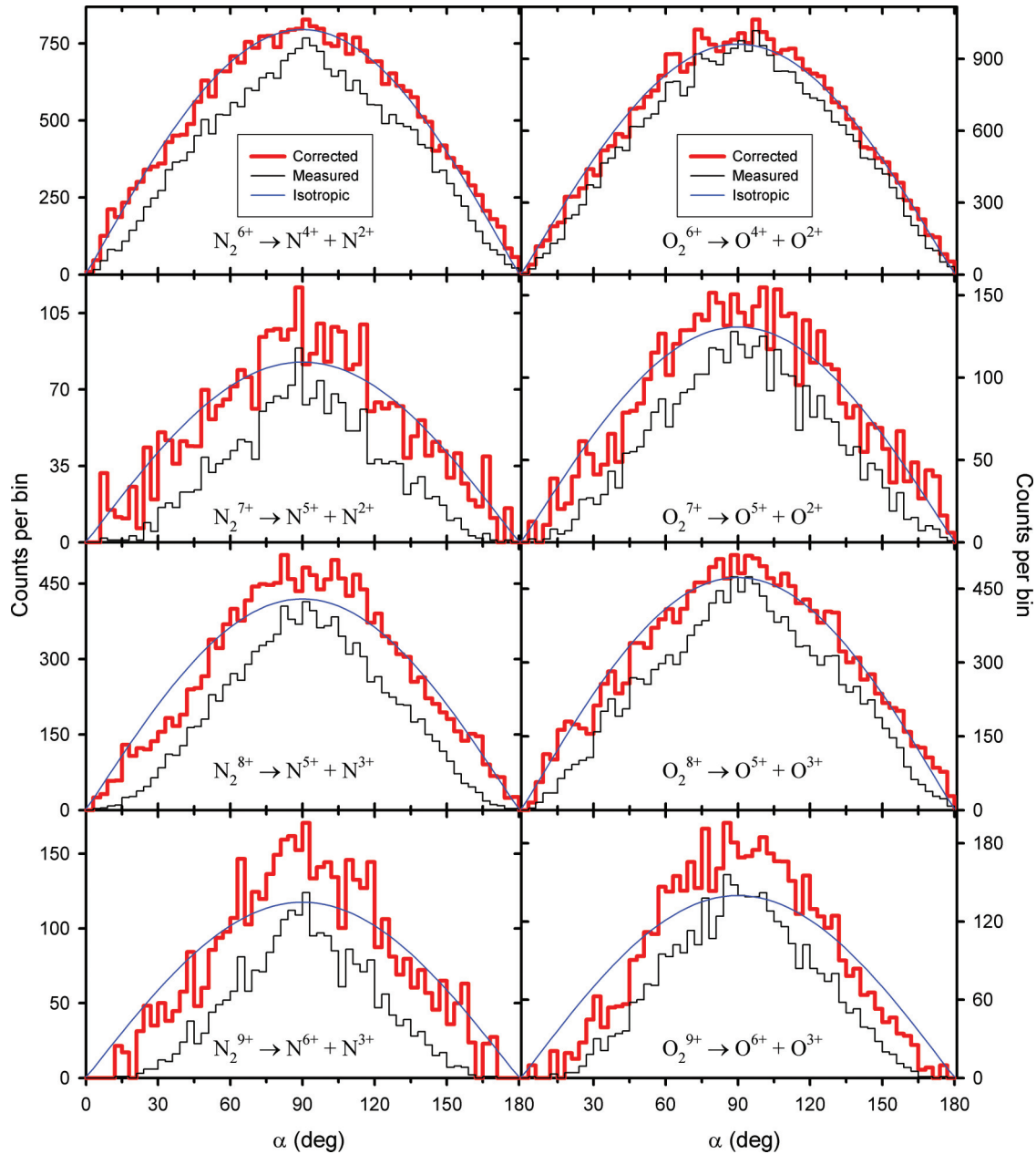


FIG. 8. (Color online) Caption identical to that of Fig. 7 applies, except that the molecular ions in each row have the same charge.

$|\cos \alpha| \leq 0.5$ in the former case and $|\cos \alpha| > 0.5$ in the latter case. For an isotropic angular distribution the two cases are expected to correspond to the same number of events. The results for the symmetric and nearly symmetric dissociation channels are shown in Fig. 9. Apparently, the molecular orientation at the time of collision does have an effect on the q_{\perp} distributions for $Q-Z > 0$ and its magnitude seems to depend on $Q-Z$. This effect was not present for the observed highly asymmetric dissociation channels.

D. Systematics of the q_{\perp} distribution most-probable values

Peak positions (or most-probable values), q_{\perp}^0 , of all the measured q_{\perp} distributions were determined as described in Sec. IV B. The results were scaled by dividing q_{\perp}^0 with A

and are shown in Fig. 10 as a function of the (parent) recoil charge-to-mass number ratio Q/A , where A is the (combined) target atomic mass number. The scaling was applied in order to produce a quantity proportional to transverse velocity, which is expected to be a universal function of Q/A for the given characteristics of the electric field experienced by the target atom or molecule during the collision.

Figure 10 shows that the peak positions q_{\perp}^0 increase as a function of Q/A , as expected, and that the results for q_{\perp}^0/A of CO are almost identical to those of N_2 , which is also expected based on the plots shown in Fig. 6 and the fact that the two gases have the same combined atomic mass number and the same combined atomic number. Furthermore, the values of q_{\perp}^0/A obtained for all molecular gases (CO, N_2 , and O_2) are found to lie very close to each other and, for the most part

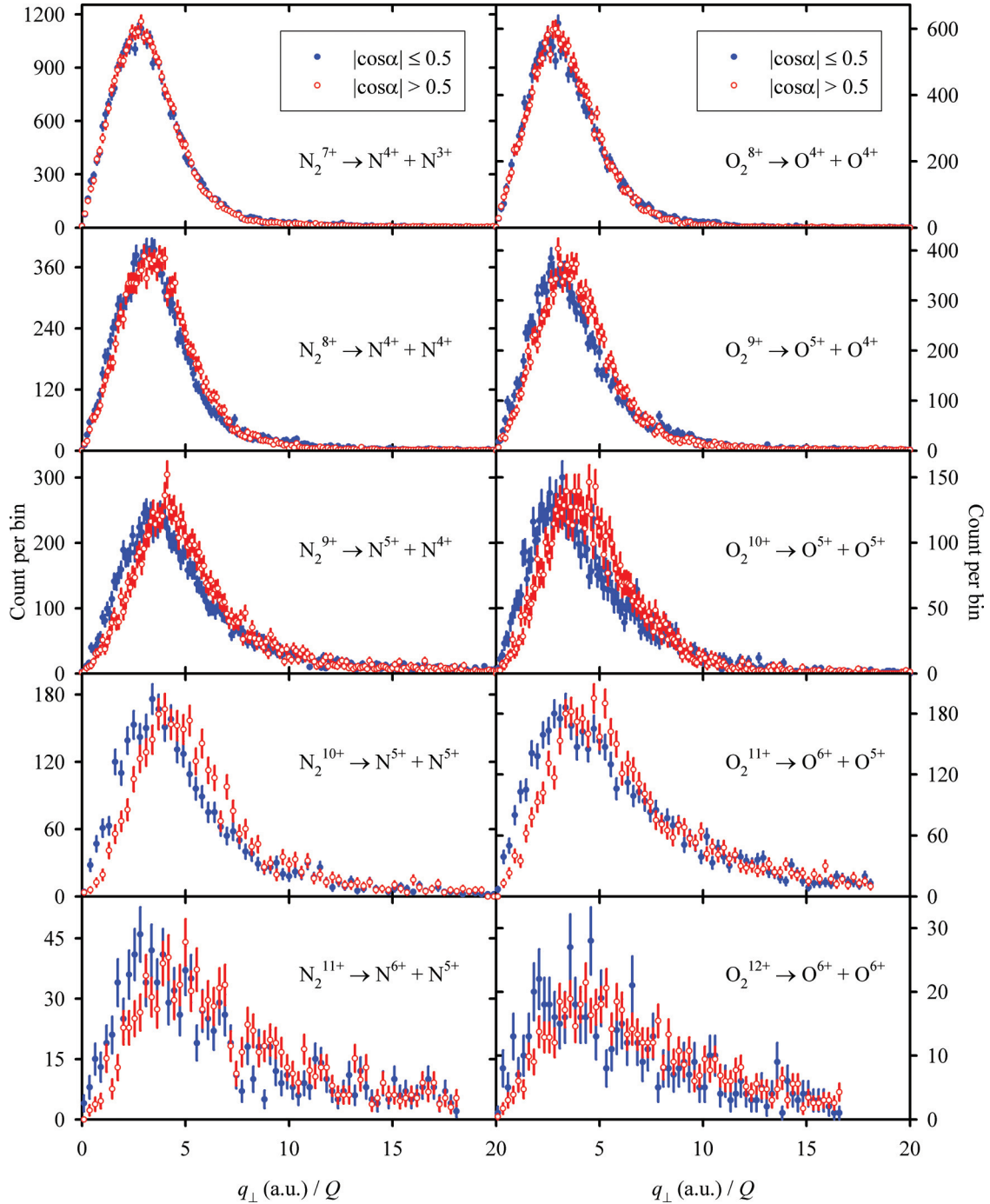


FIG. 9. (Color online) Measured q_{\perp} distributions for the selected N_2 and O_2 dissociation channels (as indicated by the labels) for angles $60^{\circ} \leq \alpha \leq 120^{\circ}$ ($|\cos \alpha| \leq 0.5$) and for the remainder of the angular range ($|\cos \alpha| > 0.5$), as indicated by the legend. The latter distribution was normalized to the total number of events of the former distribution and the scaling on the horizontal axis (i.e., division by Q) was applied to enhance the details.

(up to $Q/A = 0.33$), overlap (within the uncertainties of the results) with those obtained for Ne. For larger charge-to-mass number ratios (corresponding to charge numbers exceeding $6+$, $9+$, and $10+$ for Ne, N_2/CO , and O_2 , respectively) the results for the molecular targets seem to remain universal, but are slightly lower than those for the Ne target. On the other hand, the line connecting the results for Ar gas overlaps with the other lines only for $Q/A < 0.13$, which includes

charge states up to and including $2+$ and $5+$ for Ne and Ar, respectively.

Contrary to the expectations outlined in Sec. I, even though the molecular masses of CO, N_2 , and O_2 are about halfway in between those of Ne and Ar, the values of q_{\perp}^0/A for the molecular targets are very similar to those for Ne (for the given value of Q/A), and quite different from those for Ar, at least for large values of Q/A . As explained above, the

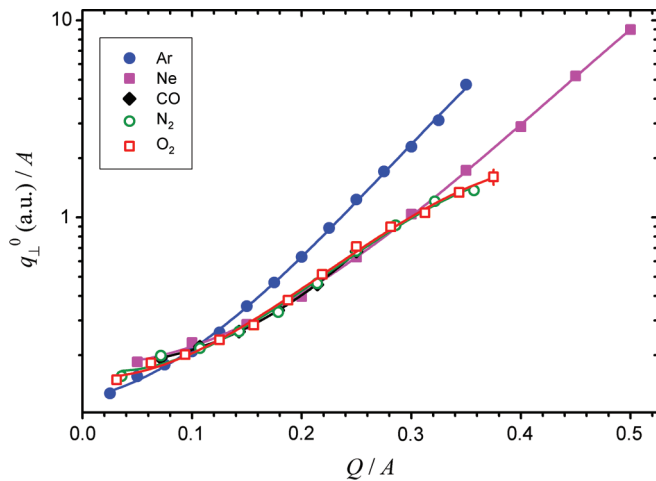


FIG. 10. (Color online) The quantity q_{\perp}^0/A plotted as a function of the charge-to-mass number ratio, shown by the symbols according to the legend. The lines represent third-order polynomial fits to the data points and are drawn to guide the eye.

differences in the results originate from the differences in the characteristics of the electric field experienced by the target atom or molecule during the collision. Apparently, for $Q/A > 0.13$, the projectile must provide a stronger electric field to Ar target atoms (compared to the other targets) in order to produce a given degree of ionization per unit mass. This means that the average impact parameter in the case of Ar target is substantially smaller than that in the case of Ne target (for the given value of $Q/A > 0.13$).

A better, although purely empirical scaling for Ar and Ne is shown in Fig. 11. It was obtained by plotting $(q_{\perp}^0/A)(Z/Q)$ versus $Q/A^{0.5}$, where Z is the target atomic number. This scaling was found to work well for $Q/A^{0.5} < 1.2$, which covers the first seven charge states of Ar and the first five charge states of Ne.

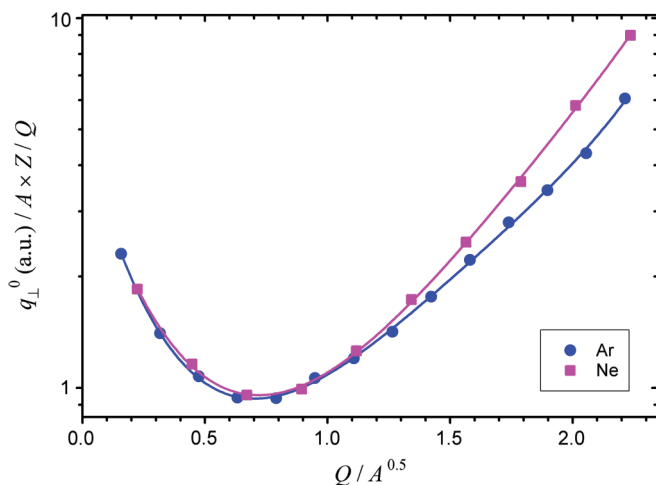


FIG. 11. (Color online) The quantity $(q_{\perp}^0/A)(Z/Q)$ plotted as a function of scaled charge-to-mass-number ratio, shown by the symbols according to the legend. The lines represent fourth-order polynomial fits to the data points and are drawn to guide the eye.

V. CONCLUSION

A recoil-ion momentum spectrometer (RIMS), featuring a skimmer-collimated effusive gas jet, fast timing, and simultaneous two-dimensional position determination capabilities, was used to measure the transverse momenta (q_{\perp}) of recoil atomic and molecular ions emerging from collisions between 2.5-MeV/u Xe^{34+} projectiles and neutral Ne, Ar, CO, N_2 , and O_2 gases as a function of the degree of target ionization. For the molecular targets the distributions of q_{\perp} corresponding to different dissociation channels were separated. Measurements with all the targets were performed under virtually identical conditions, so that the results could be directly compared in detail.

The measured q_{\perp} distributions are characterized by single, generally asymmetric peaks and, at least in the region covered by the full width at half maximum, they can be well described by a Weibull function, so that their most-probable values can be determined precisely and consistently. Except for the argon target, the velocities corresponding to the maxima of the distributions were found to follow (within the uncertainties of the results) a universal function of the target charge-to-mass number ratio for values up to 0.33, which covers charge states up to and including $6+$, $9+$, and $10+$ for Ne, N_2/CO , and O_2 , respectively. For larger charge-to-mass number ratios the results for the molecular targets appear to remain universal, but are slightly different from the results for the neon target. A more elaborate scaling was required to obtain a universal function that describes the results for neon and argon targets in a similar way. The universality was found to cover only the first seven charge states of argon and the first five charge states of neon.

It was also found that for a given molecular target the q_{\perp} distributions are essentially the same for all dissociation channels corresponding to the same combined fragment charge number Q , as long as $Q < 7$, so that tightly bound electrons are not likely to be removed and pure ionization is the dominant mechanism for electron removal. However, for different dissociation channels of the same parent molecular ion with charge state exceeding $6+$, it was found that q_{\perp} distributions are shifted toward higher values for the more asymmetric dissociation channels and increasingly so as the degree of target ionization increases. This effect was explained by the differences in the impact parameter distributions between the two most-likely ionization mechanisms, i.e., pure ionization and ionization accompanied by electron transfer from the target to the projectile, the latter being more prominent for the more asymmetric dissociation channel. An additional explanation for this effect pointed to the fact that a less asymmetric dissociation channel typically corresponds to a lower value of the ionization potential, which is also part of the reason why a less asymmetric dissociation channel is more prominent.

The distributions of q_{\perp} for CO or N_2 recoil ions of a given final charge $Q \leq 7$ were found to be practically the same, which is not surprising since the two molecules have the same combined atomic mass numbers and the same combined atomic numbers.

For the present collision regime no conclusive evidence was found for anisotropy in the angular distributions of fragments from low-charged molecular ions produced in

the collisions. However, for the symmetric and the nearly symmetric dissociation channels the fragments with combined charge number Q exceeding 9 for N_2 and 10 for O_2 were found to be distributed with a reduced probability at angles close to 90° relative to the beam direction. Furthermore, the effect was found to become more significant as Q increases and to depend on the number of electrons removed in addition to one half of the number of available electrons ($Q-Z$). On the other hand, for highly asymmetric dissociation channels the angular distributions seem to indicate that the fragments of highly charged molecular ions may be distributed with an enhanced probability at angles close to 90° relative to the beam direction. The magnitude of this effect was found to be very small, as expected.

A small molecular orientation effect on the q_\perp distributions was observed for symmetric and nearly symmetric dissociation channels having $Q-Z > 0$. Its magnitude also seems to depend on $Q-Z$.

Hopefully, the features presented in this paper will stimulate the development of theoretical models and simulations capable of handling rather complex systems such as those studied in this work, with special emphasis on molecular targets.

ACKNOWLEDGMENT

This work was supported by Grant No. A-0355 from the Robert A. Welch Foundation.

-
- [1] C. L. Cocke and R. E. Olson, *Phys. Rep.* **205**, 153 (1991).
- [2] J. Ullrich, R. Moshhammer, R. Dörner, O. Jagutzki, V. Mergel, H. Schmidt-Böcking, and L. Spielberger, *J. Phys. B* **30**, 2917 (1997).
- [3] R. Dörner, V. Mergel, O. Jagutzki, L. Spielberger, J. Ullrich, R. Moshhammer, and H. Schmidt-Böcking, *Phys. Rep.* **330**, 95 (2000).
- [4] J. Ullrich, R. Moshhammer, A. Dorn, R. Dörner, L. Ph. H. Schmidt, and H. Schmidt-Böcking, *Rep. Prog. Phys.* **66**, 1463 (2003).
- [5] M. Schulz and D. H. Madison, *Int. J. Mod. Phys. A* **21**, 3649 (2006).
- [6] <http://www.roentdek.com>
- [7] T. J. Gray, C. L. Cocke, and E. Justiniano, *Phys. Rev. A* **22**, 849 (1980).
- [8] M. Unverzagt, R. Moshhammer, W. Schmitt, R. E. Olson, P. Jardin, V. Mergel, J. Ullrich, and H. Schmidt-Böcking, *Phys. Rev. Lett.* **76**, 1043 (1996).
- [9] P. Jardin, A. Cassimi, J. P. Grandin, D. Hennecart, and J. P. Lemoigne, *Nucl. Instrum. Methods Phys. Res., Sect. B* **107**, 41 (1996).
- [10] V. Frohne, S. Cheng, R. M. Ali, M. L. A. Raphaelian, C. L. Cocke, and R. Olson, *Phys. Rev. A* **53**, 2407 (1996).
- [11] V. Horvat and R. L. Watson, *Nucl. Instrum. Methods Phys. Res., Sect. B* **269**, 2584 (2011).